

# Nanoscale

Accepted Manuscript



This is an *Accepted Manuscript*, which has been through the Royal Society of Chemistry peer review process and has been accepted for publication.

*Accepted Manuscripts* are published online shortly after acceptance, before technical editing, formatting and proof reading. Using this free service, authors can make their results available to the community, in citable form, before we publish the edited article. We will replace this *Accepted Manuscript* with the edited and formatted *Advance Article* as soon as it is available.

You can find more information about *Accepted Manuscripts* in the [Information for Authors](#).

Please note that technical editing may introduce minor changes to the text and/or graphics, which may alter content. The journal's standard [Terms & Conditions](#) and the [Ethical guidelines](#) still apply. In no event shall the Royal Society of Chemistry be held responsible for any errors or omissions in this *Accepted Manuscript* or any consequences arising from the use of any information it contains.



Cite this: DOI: 10.1039/xxxxxxxxxx

# Emission enhancement and polarization of semiconductor quantum dots with nanoimprinted plasmonic cavities: towards scalable fabrication of plasmon-exciton displays †

Jasper J. Cadusch,<sup>a\*</sup> Evgeniy Panchenko,<sup>a</sup> Nicholas Kirkwood,<sup>b</sup> Timothy D. James,<sup>a,c</sup> Brant C. Gibson,<sup>d</sup> Kevin J. Webb,<sup>e</sup> Paul Mulvaney,<sup>b</sup> and Ann Roberts<sup>a</sup>

Received Date  
Accepted Date

DOI: 10.1039/xxxxxxxxxx

www.rsc.org/journalname

## Abstract

Here we present an application of a high throughput nanofabrication technique to the creation of a plasmonic metasurface and demonstrate its application to the enhancement and control of radiation by quantum dots (QDs). The metasurface consists of an array of cold-forged rectangular nanocavities in a thin silver film. High quantum efficiency graded alloy CdSe/CdS/ZnS quantum dots were spread over the metasurface and the effects of the plasmon-exciton interactions characterised. We found a four-fold increase in the QDs radiative decay rate and emission brightness, compared to QDs on glass, along with a degree of linear polarisation of 0.73 in the emitted field. Such a surface could be easily integrated with current QD display or organic solar cell designs.

## Introduction

Quantum dot (QD) displays offer several advantages over conventional display technologies. QD displays offer richer color gamuts, higher resolution and consume less than a fifth of the energy of current LCD screens,<sup>1</sup> which could lead to longer portable device battery life. At the same time, with the rise of 3D films and sophisticated home entertainment systems, polarisation-based

3D display technologies are gaining in popularity. Widespread availability of 3D visualisation technologies will also prove useful in medical, industrial design and 'big data' settings.

The weak coupling of excited quantum states to cavity modes can lead to emission enhancement via the Purcell effect,<sup>2</sup> which then allows for devices with a higher external quantum efficiency (EQE) and lower power consumption. To achieve enhanced and polarised emission from quantum sources, photonic or plasmonic interactions have previously been investigated.<sup>3–7</sup> Plasmonic designs have the advantage of being highly compact and readily integrable with current QD display designs.

Precisely fabricated plasmonic devices have been used to demonstrate enhancement of the directivity, polarisation and intensity of QD emission.<sup>8,9</sup> These approaches, however, rely on slow and costly fabrication techniques such as electron beam lithography or focused ion beam milling. Here we demonstrate an application of a cost-effective, high throughput, scalable nanofabrication technique, known as resistless nanoimprint lithography (RNIL) or cold forging.<sup>10</sup> Using this technique we demonstrate both radiative decay rate enhancement and control of emission polarisation due to the interaction of quantum dot excitons with the plasmonic modes of an array of nanocavities.

RNIL allows for rapid fabrication of metallic nanostructures and could lead to large scale implementation of plasmonic devices. Unlike nanoimprint lithography with polymer resists, cold forging, as the name suggests, does not require high temperatures for successful pattern replication. The result is the imprinting cycle times and the total fabrication costs are greatly reduced. The process, shown in Fig. 1, consists of two steps; (I) fabrication of a master template and (II) imprinting of the

<sup>a</sup> School of Physics, The University of Melbourne, Parkville, VIC 3010, Australia; E-mail: jcadusch@student.unimelb.edu.au

<sup>b</sup> School of Chemistry and Bio21 Institute, The University of Melbourne, Parkville, VIC 3010, Australia.

<sup>c</sup> Melbourne Centre for Nanofabrication (MCN), Australian National Fabrication Facility, Clayton, VIC, 3168, Australia.

<sup>d</sup> College of Science, Engineering and Health, RMIT University, Melbourne, VIC, 3001, Australia.

<sup>e</sup> School of Electrical and Computer Engineering, Purdue University, West Lafayette, IN, 47907, USA.

† Electronic Supplementary Information (ESI) available: [details of any supplementary information available should be included here]. See DOI: 10.1039/b000000x/

master into the target substrate. Typically, the master is a silicon wafer, patterned using nanolithographic techniques, then pressed into a silver, aluminium or gold film on a silicon or glass substrate.

Previously,<sup>10,11</sup> the spectral response of plasmonic cavities created with RNIL and other methods,<sup>12</sup> showed surprisingly sharp and short wavelength resonances, compared to apertures of similar dimensions.<sup>13</sup> The modes supported by these nanocavities have a node of the electric field near the metallic end of the cavity and an antinode at the open end.<sup>†</sup> This fact permits strong blue resonances in the nanocavities, something that is critical to color displays, is difficult to achieve with nanoapertures and is a major issue for current organic LED (OLED) based displays.

Plasmonic enhancement of quantum sources is usually realised using so called ‘top-down’ techniques, such as focused ion beam milling or electron beam lithography. This allows precise fabrication of plasmonic devices with good geometric control. One drawback of current top down nanofabrication techniques, however, is the low throughput and the associated high cost per unit. Nanoimprint lithography was introduced in 1995 to address these concerns.<sup>14</sup> The nanoimprint process usually employs either a UV curable resist or a polymer which is thermally softened, then the desired pattern imprinted. An additional metal deposition and etching or lift off step is required to create the metallic nanostructures needed for plasmonics. Resistless nanoimprint lithography,<sup>10</sup> however, permits direct patterning of metallic films without the need for heating or UV exposure. A master template is fabricated using electron beam lithography, then pressed into a metallic ‘target’ film. The dimensions of the pattern to be transferred to the metal film appears to be limited only by the resolution of the EBL step. By eliminating the need for heating and cooling or UV curing of substrates, the duty cycle time of a RNIL process can be fractions of a second, allowing for rapid and repeatable high throughput nanofabrication. Because of the high fidelity, high throughput and low cost of this process it is well suited for use in future industrialised nanotechnologies. The cold forging process used here is illustrated in Fig. 1.

## Fabrication and Experimental Methods

We prepared the plasmonic nanocavities using resistless nanoimprint lithography.<sup>10</sup> To create the master template, a 40 nm layer of hydrogen silsesquioxane (HSQ) electron beam resist was spin-coated onto a 100 mm  $\times$  100 mm p-type Si wafer, then baked at 150°C for 3 minutes. The pattern to be imprinted was then exposed using a Vistech EBPG 5000+ 100 kV electron beam lithography system. After removing the unexposed HSQ by developing the wafer in AZ 726 for 1 minute, the Si wafer was etched using a reactive ion etch (Oxford Instruments PlasmaLab100 ICP380 RIE). A 5/30 sccm Ar/Cl<sub>2</sub> plasma etch chemistry was used for 45 seconds to etch the master template to 150 nm deep. Target Ag films were prepared using a IntVac NanoChromeII electron beam deposition system. A 360 nm thick Ag film was evaporated onto a Si substrate, with a 2 nm Ge adhesion layer between the Si and Ag. A proprietary silanised perfluorinated hydrocarbon-based anti-sticking layer, (EVG), was

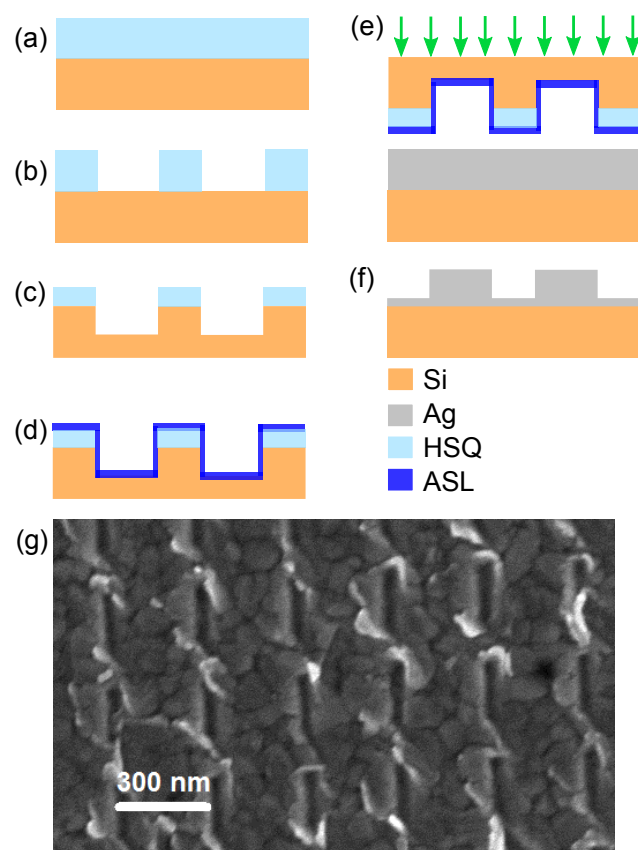


**Fig. 1** A depiction of the resistless nanoimprinting process. A 40 nm layer of HSQ is spun onto a silicon wafer (a), which is patterned using EBL (b) and etched using RIE (c), an anti-sticking layer is applied to the master (d), then pressure is applied to force the master into a silver film (e). The inverse pattern is now imprinted into the silver film (f). A scanning electron micrograph (g) of the resistless nanoimprinted cavity array in a silver film. The cavities are highly asymmetric, measuring 200 nm long by 40 nm wide.

applied to the Si master template to reduce adhesion of the metal film to the master and increase the lifetime of the master template. An EVG 520S Hot Embosser was used to perform the cold forging step. The Si master and Ag film were stacked in the chamber with a 5 mm thick titanium top plate. The chamber was evacuated to 1 mbar and 2.49 MPa pressure was applied to the wafer stack for 5 minutes, with a slew rate of 64 kPa/min. After imprinting, the Si master can be re-used approximately 8 times before the nanofeatures are degraded by wear. This issue can be overcome by substituting the Si master for one composed of Ni, which has been shown to imprint high fidelity patterns even after 8000 imprint cycles.<sup>15</sup> The resulting nanocavities are shown in the scanning electron micrograph in Fig. 1(g). The rectangular nanocavities are 40 nm wide and 200 nm long, with an array period of 300 nm. Atomic force microscopy reveals the cavity depth to be approximately 40 nm  $\pm$  3 nm. Excess metal from the nanocavities is squeezed out to the side, where the cast off can be seen as the bright areas around the cavities in Fig. 1(g).

The spectral emission properties of semiconductor nanocrystals

or quantum dots, such as emission wavelength and linewidth, as well as intensity, can be tailored during the growth process. Due to their small size, high brightness and relative stability, quantum dots are an attractive solution for some of the challenges of modern photonics, such as solar energy harvesting,<sup>16</sup> telecommunication and energy efficient illumination.<sup>17</sup> QDs are also readily integrable with plasmonic structures, which allows for further control over their emission properties, such as beam steering,<sup>18</sup> polarisation or radiative decay rate enhancement.<sup>19</sup>

The quantum dots used here consisted of a 4.5 nm diameter CdSe core with a 6 nm thick graded alloy  $\text{Cd}_x\text{Zn}_{1-x}\text{S}$  shell.<sup>20</sup> The final QD diameters were normally distributed about  $10 \text{ nm} \pm 2 \text{ nm}$ . Due to the small variation in QD size, the absorption and decay properties of each QD in this sample were similar. The growth process is detailed elsewhere.<sup>20</sup> At the time of growth these QDs exhibited an 80% quantum efficiency, and a mean lifetime of 17 ns in a 15 micromol concentrated solution, with hexane as the solvent.

To incorporate the quantum dots with the nanoimprinted metasurface, the QDs were mixed with SU8 2000.5 to provide environmental stability. The final QD concentration in the SU8 film was  $1.4 \mu\text{mol}$ . The SU8/QD mixture was then drop-cast onto the patterned silver film and sealed with a glass cover slip. The SU8 was then cured under UV light. The SU8 layer thickness of  $12 \mu\text{m}$  was determined using confocal microscopy.

Fluorescence scans were performed using a Nikon Ti-80i inverted microscope fitted with a 100x 1.3 NA oil immersion lens, a Perkin Elmer SPCM-AQRH-14-FC avalanche photo diode (APD) and a Mad City Labs NanoDrive xy piezo stage. Fluorescent spectra and the nanocavity reflectance spectrum were measured using an Andor Solis cooled spectrograph CCD array. Fluorescent lifetime measurements were carried out using the time correlated single photon counting (TCSPC) technique using a synchronised Picoquant TimeHarp 200 and the APD. Information about the quantum dot radiative lifetime and decay rate distribution was retrieved by fitting an exponential decay weighted by a log normal distribution to the TCSPC data.<sup>21</sup> The light source used for these measurements was an NKT SuperK supercontinuum photonic crystal fiber laser, with a 10 MHz repetition rate. The broadband light was filtered with a high optical density  $531 \text{ nm} \pm 11 \text{ nm}$  bandpass filter (531/22 Brightline) and a 531 nm longpass dichroic beamsplitter (532 nm Brightline Laser Dichroic Beamsplitter), resulting in a spatially coherent pumping spectrum of 532 nm to 540 nm. The reflected light from the sample was then collected from the dichroic beamsplitter through a 532 nm long pass filter (532 nm RazorEdge LWP) and focused onto the APD. The range of wavelengths detectable with this set up is 541 nm to 1100 nm.

## Results and discussion

The measured cavity reflectance spectrum, shown in Fig. 2, has a dip in reflection at a wavelength of 670 nm, with a full-width-at-half-maximum of 70 nm. This can be attributed to the excitation

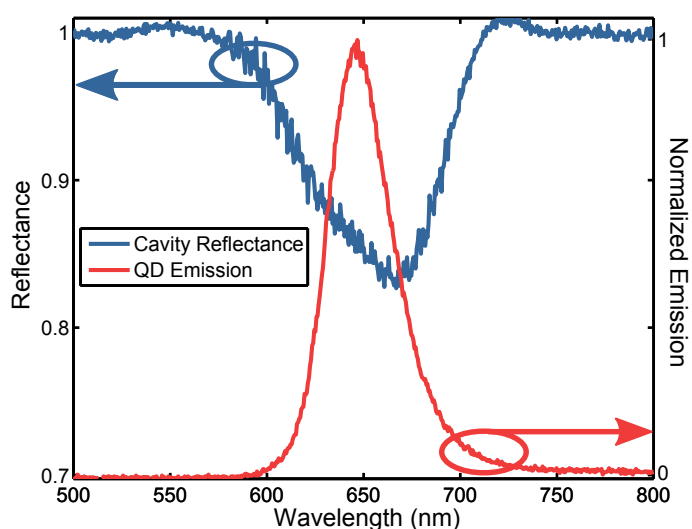


**Fig. 2** The measured reflectance of the SU8 encapsulated silver nanocavity array (blue line) and the normalized emission from the  $\text{Cd}_x\text{Zn}_{1-x}\text{S}$  quantum dots in SU8, measured on a glass microscope slide (red line).

of the fundamental cavity mode, which is broadened due to irregularities in the fabricated cavity dimensions. Fig. 2 also shows the fluorescence spectrum of the  $\text{Cd}_x\text{Zn}_{1-x}\text{S}$  QDs. The pump laser excites the quantum dot excitons and these decay with a peak emission wavelength of 645 nm. The QD emission band overlaps with the fundamental resonant mode of the nanocavities, which permits weak coupling between the QD excited state and the plasmonic cavity mode. The bright regions in the scanning fluorescence image shown in Fig. are from quantum dots located in close proximity to the plasmonic nanocavities, where the interaction between plasmons and excitons is strongest. The fine details (text, outline, and wings) in Fig. are dimmer than central parts as they are only one or two nanocavities wide<sup>†</sup>, so the overall intensity sampled by the microscope objective is lower in these regions. The plasmon-exciton coupling leads to a two-fold increase in the intensity of the collected light, compared to the background fluorescence of the QDs on the Ag film and a 95% increase in the external quantum efficiency<sup>†</sup> of the device. This is a manifestation of the Purcell effect, where the introduction of extra radiative decay pathways (that is, an increase in the local density of optical states), via coupling of the QD excitons to plasmon cavity modes, has greatly increased the excited state decay rate, so we collect more photons per unit time when the QDs interact with the plasmonic nanocavities. This enhancement effect is on top of any Purcell enhancement afforded by the unpatterned Ag film and the SU8 encapsulation layer.

Scanning the sample and collecting spectra with an analyser at  $0^\circ$  and  $90^\circ$  to the long axis of the nanocavities, reveals the emitted light near the imprinted cavities has a preferential polarisation direction perpendicular to the long axis of the cavities, whereas light from QDs away from the cavities is unpolarised. This is consistent with the excitation of the cavity mode that has this polarisation. By comparing the recorded intensities for both polarisation states, the degree of linear polarisation (DOLP) can

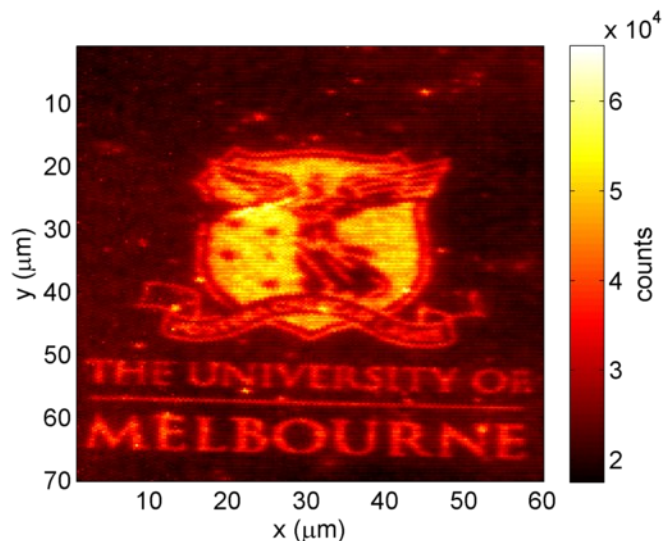


**Fig. 3** A fluorescence microscope scan of the quantum dots interacting with the nanoimprinted cavities. The emission from QDs near the cavities have around 3.5 times the intensity than for QDs near the bare Ag film. This is evidence of coupling between the plasmonic cavity modes and the quantum dot excitons.

be calculated. The spatial variation of the DOLP is shown in Fig. 4, with a maximum value of 0.73 from the cavity array. The measured value is reduced due to the presence of ‘spectator’ QDs throughout the 12  $\mu\text{m}$  thick SU8 film, as identified using confocal microscopy. Quantum dots more than 5  $\mu\text{m}$  above the cavities do not appear to behave differently to QDs the same height above the unpatterned film<sup>†</sup>. We reason that the value of the degree of linear polarisation could be increased by using a much thinner ( $\sim 30$  nm) film of QDs, as would be found in a commercial QD display.

The time correlated single photon counting histograms shown in Fig. 5(a) have been normalised so that the maximum count is one. This allows for easy comparison of QD lifetimes for the 3 environments; in SU8 on glass, in SU8 on the unpatterned silver film and in SU8 on the nanoimprinted metasurface. Each histogram can be thought of as a probability density function,  $f(t)$ , representing the probability of detecting a photon at some time,  $t$ , after the excitation pulse. For a single emitter, with a single excited state,  $f(t)$  will be an exponential decay;  $f(t) = e^{-\Gamma t}$ , where the decay rate,  $\Gamma = 1/\tau$  and  $\tau$  is the excited state lifetime. To fit the decay characteristics for more realistic cases with an ensemble of different emitters, each with multiple excited states, a stretched exponential is a popular choice for  $f(t) = e^{-(\Gamma t)^\beta}$ .<sup>20</sup> Here, we will follow the lead of van Driel *et al.*,<sup>21</sup> and model the lifetime distribution using

$$f(t) = \int_0^\infty e^{-\Gamma t} \sigma(\Gamma) d\Gamma, \quad (1)$$

where  $\sigma(\Gamma)$  represents the distribution of total decay rates of, in this case, multiple quantum dots. We model the decay rate distribution function,  $\sigma(\Gamma)$ , as a lognormal distribution so that

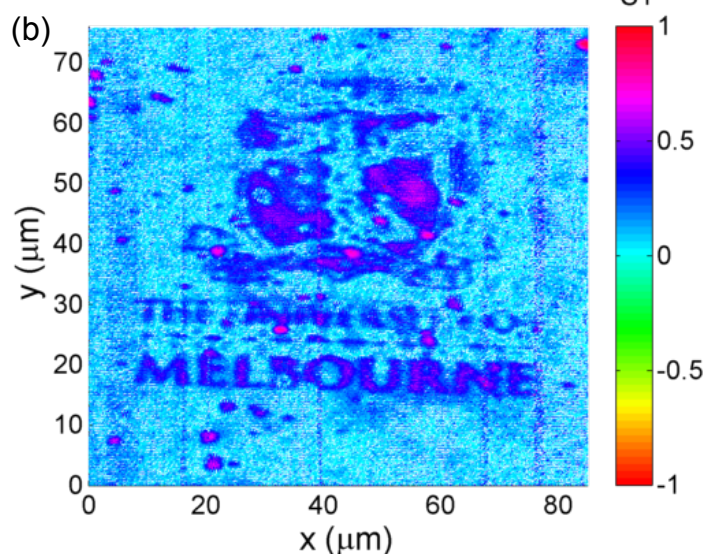
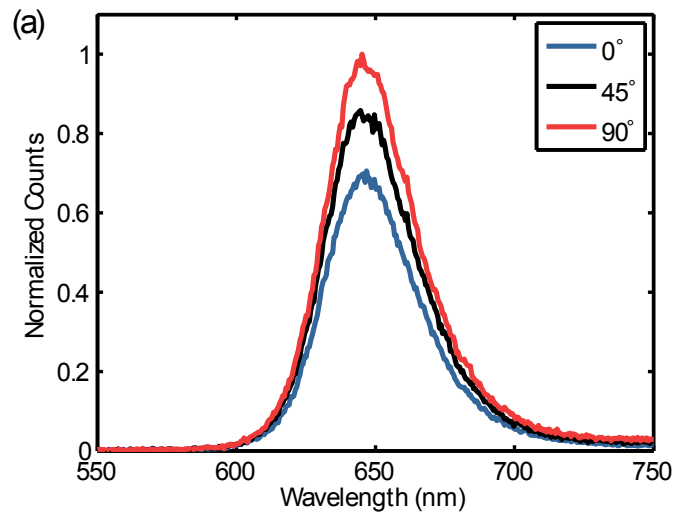


**Fig. 4** Normalised emission spectra (a) for the cavity coupled quantum dots with an analyser at  $0^\circ$  (blue),  $45^\circ$  (black) and  $90^\circ$  (red) to the long axis of the nanocavities. (b) the spatial distribution of the degree of linear polarisation, or S1, of the QD emission. The value of S1 for light collected above the cavities is up to 0.73, whilst over the Ag film it is 0.

$$\sigma(\Gamma) = \frac{1}{\Gamma_m w \sqrt{\pi} e^{-\frac{w^2}{4}}} e^{-\left(\frac{\ln \Gamma - \ln \Gamma_m}{w}\right)^2}, \quad (2)$$

where  $\Gamma_m$  is the most frequent total decay rate and  $w$  is related to  $\Delta\Gamma$ , the width of the distribution, by  $\Delta\Gamma = 2\Gamma_m \sinh(w)$ .<sup>19</sup> The advantage of using this analysis of the decay behavior of the QD excitons compared to the stretched exponential approach is that  $\Gamma_m$  and  $\Delta\Gamma$  can easily be physically interpreted, whereas  $\beta$  does not have a straightforward physical interpretation.<sup>21</sup>

To fit  $f(t)$  using equations (1) and (2), to the TCSPC data shown in Fig. 5(a), a cost function approach was employed to find the values of  $\Gamma_m$  and  $w$  that minimise the difference between the measured data and  $f(t)$  over the 35 ns measurement window. Once  $\Gamma_m$  and  $w$  have been estimated, we can generate the total decay rate distribution functions,  $\sigma(\Gamma)$ , find  $f(t)$  and

then calculate the expected lifetime using,

$$\tau = \int_0^{\infty} t f(t) dt. \quad (3)$$

The total decay rate distributions calculated from the TCSPC data using equations (1) and (2) are shown in Fig. 5(b), normalized to their peak values,  $\sigma_{max}$ . For the case of the graded alloy quantum dots suspended in cured SU8 on a glass substrate, we found the mean lifetime,  $\tau$  to be 17.4 ns with a most frequent total decay rate,  $\Gamma_m$  of 0.07 per ns. For QDs on the unpatterned silver film, we found an average lifetime of 14.4 ns and a  $\Gamma_m$  of 0.138 per ns. For QDs interacting with the nanoimprinted metasurface, the lifetime was reduced to 3.9 ns and the most frequent exciton decay rate increased to 0.237 per ns. By comparing the lifetime values for quantum dots in SU8 on glass,  $\tau_0$ , and near the nanocavities,  $\tau_c$ , we can estimate the Purcell enhancement factor,  $F_p = \frac{\Gamma_c}{\Gamma_0} = \frac{\tau_0}{\tau_c}$ , of this scalable metasurface to be  $F_p = 4.46$ . This enhancement factor agrees with the measured increase in QD brightness near the plasmonic nanocavities in Fig. .

The Purcell factor associated with the nanoimprinted metasurface can be increased by fine tuning of the cavity dimensions to increase the spectral overlap of the exciton and cavity frequencies. Further improvement can be achieved by reducing the plasmon damping in the cavity by reducing the crystal grain sizes of the Ag film and more precise control of QD position. That being said, the Purcell factor and associated polarisation of emission demonstrated here, with this cost effective technique, compares favorably with previously reported enhancements using direct write approaches.<sup>22</sup> Work still to be done includes designing and fabricating a metasurface that will impose a particular circular polarisation on the QD emission, which is superior for use in 3D display technologies compared to linearly polarised light. This can be achieved by tailoring multipolar plasmon modes,<sup>23</sup> or with a chiral metasurface.<sup>24</sup>

## Conclusions

Here we have demonstrated an application of a robust and scalable nanofabrication technique for creating plasmonic nanocavity arrays in metallic films. Applying a monodisperse solution of CdSe/CdS/ZnS graded alloy quantum dots suspended in cured SU8 to a nanoimprinted metasurface resulted in nearly a 4-fold enhancement in radiative decay rate and brightness, as well as a high degree of linear polarisation of the emission close to 0.73. This technique will prove useful in the development of polarised QD displays, QD based light harvesting and photodetection as well as being extended for use in telecommunication and photonic computing applications. Current work is focused on a systematic study of the nanocavity parameter space.

## Acknowledgements

This work was performed in part at the Melbourne Centre for Nanofabrication (MCN) in the Victorian Node of the Australian National Fabrication Facility (ANFF). This research was supported under the Australian Research Council's Discovery Projects funding scheme (project number DP110100221) and a Melbourne Centre for Nanofabrication Technical Fellowship.

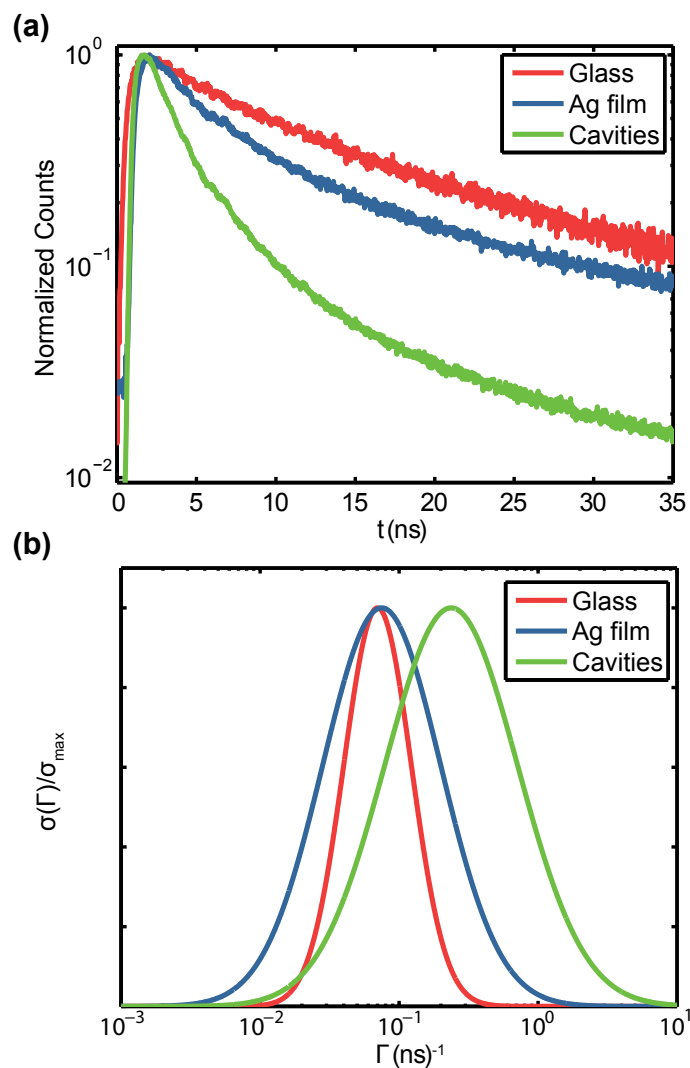


**Fig. 5** (a) Normalised TCSPC histograms for quantum dots in SU8 from the same batch on glass (red) with  $\tau = 17.4$  ns, on the bare silver film (blue)  $\tau = 14.4$  ns and on the nanoimprinted cavity array (green)  $\tau = 3.9$  ns. It is clear that plasmon-exciton interactions lead to a greatly reduced radiative lifetime. (b) The calculated total decay rate distributions  $\sigma(\Gamma)$ , normalized to their peak values,  $\sigma_{max}$ , for quantum dots in SU8 on glass (red), on an unpatterned silver film (blue) and on nanoimprinted cavities (green). The mean decay rate increases from  $\Gamma_m = 0.07$  per ns for QDs on glass to  $\Gamma_m = 0.237$  per ns for the cavity coupled QDs, an increase of three and a half times. The spread of the decay rate distribution also increases from  $\Delta\Gamma = 0.14$  per ns for QDs on glass to  $\Delta\Gamma = 0.56$  per ns for cavity coupled QDs.

## References

- 1 J. H. Oh, K.-H. Lee, H. C. Yoon, H. Yang and Y. R. Do, *Optics Express*, 2014, **22**, A511–A520.
- 2 E. M. Purcell, *Physical Review*, 1946, **69**, 681.
- 3 A. Akimov, A. Mukherjee, C. Yu, D. Chang, A. Zibrov, P. Hemmer, H. Park and M. Lukin, *Nature*, 2007, **450**, 402–406.
- 4 T. James, Z. Teo, D. Gomez, T. Davis and A. Roberts, *Applied Physics Letters*, 2013, **102**, 033106.
- 5 D. Englund, D. Fattal, E. Waks, G. Solomon, B. Zhang, T. Nakaoka, Y. Arakawa, Y. Yamamoto and J. Vučković, *Physical review letters*, 2005, **95**, 013904.
- 6 K. Tanaka, E. Plum, J. Ou, T. Uchino and N. Zheludev, *Physical Review Letters*, 2010, **105**, 227403.
- 7 N. Ganesh, W. Zhang, P. C. Mathias, E. Chow, J. Soares, V. Malyarchuk, A. D. Smith and B. T. Cunningham, *Nature Nanotechnology*, 2007, **2**, 515–520.
- 8 L. Novotny and N. Van Hulst, *Nature Photonics*, 2011, **5**, 83–90.
- 9 J.-H. Song, T. Atay, S. Shi, H. Urabe and A. V. Nurmikko, *Nano letters*, 2005, **5**, 1557–1561.
- 10 L. T. Varghese, L. Fan, Y. Xuan, C. Tansarawiput, S. Kim and M. Qi, *Small*, 2013, **9**, 3778–3783.
- 11 S. Kim, Y. Xuan, V. P. Drachev, L. T. Varghese, L. Fan, M. Qi and K. J. Webb, *Optics Express*, 2013, **21**, 15081–15089.
- 12 J. Zhang, J. Ou, K. MacDonald and N. Zheludev, *Journal of Optics*, 2012, **14**, 114002.
- 13 J. J. Cadusch, T. D. James and A. Roberts, *Optics Express*, 2013, **21**, 28450–28455.
- 14 S. Y. Chou, P. R. Krauss and P. J. Renstrom, *Journal of Vacuum Science & Technology B*, 1996, **14**, 4129–4133.
- 15 Y. Zhou, M. Asbahi, G. Luo, T. Eriksson, S. Yamada, P. V. Krishnan and B. Heidari, *SPIE Advanced Lithography*, 2010, pp. 76371X–76371X.
- 16 A. Nozik, *Physica E: Low-dimensional Systems and Nanostructures*, 2002, **14**, 115–120.
- 17 B. S. Mashford, T.-L. Nguyen, G. J. Wilson and P. Mulvaney, *Journal of Materials Chemistry*, 2010, **20**, 167–172.
- 18 A. Djalalian-Assl, D. Gomez, A. Roberts and T. Davis, *Optics Letters*, 2012, **37**, 4206–4208.
- 19 D. Ratchford, K. Działkowski, T. Hartsfield, X. Li, Y. Gao and Z. Tang, *Journal of Applied Physics*, 2011, **109**, 103509.
- 20 K. Boldt, N. Kirkwood, G. A. Beane and P. Mulvaney, *Chemistry of Materials*, 2013, **25**, 4731–4738.
- 21 A. Van Driel, I. Nikolaev, P. Vergeer, P. Lodahl, D. Vanmaekelbergh and W. Vos, *Physical Review B*, 2007, **75**, 035329.
- 22 H. Mertens and A. Polman, *Applied Physics Letters*, 2006, **89**, 211107.
- 23 S. S. Kruk, M. Decker, I. Staude, S. Schlecht, M. Greppmair, D. N. Neshev and Y. S. Kivshar, *ACS Photonics*, 2014, **1**, 1218–1223.
- 24 J. J. Cadusch, T. D. James, A. Djalalian-Assl, T. J. Davis and A. Roberts, *Photonic Technology Letters*, 2014, **26**, 2357–2360.